Photocatalytic Oxidation of SO_2 from Flue Gas in the Presence of Mn/Copper Slag as a Novel Nanocatalyst: Optimizations by Box-Behnken Design

Rabiee, Fattah; Mahanpoor, Kazem*[+]

Department of Chemistry, Arak Branch, Islamic Azad University, P.O. Box Box 38135-567 Arak, I.R. IRAN

ABSTRACT: *One of the principal air pollutants is sulfur dioxide (SO_2). The removal of SO_2 from flue gas has been one of the key challenges in the control of SO_2 emission. In this work, experimental scale photocatalytic oxidation of SO_2 is a major process leading to H_2SO_4 as a new method was suggested on the Liquid phase using Manganese supported on Copper Slag (Mn/CS) under UltraViolet (UV) irradiation. Mn/CS recognized as a novel nanocatalyst for photocatalytic oxidation of SO_2 from simulated flue gas. In this study, a Column Packed Photo Catalytic Reactor (CPPCR) was applied. Firstly, the Mn/CS was perpetrated by the impregnation method. Analysis of X-Ray Diffraction (XRD), Field Scanning Electron Microscopy (FESEM), Energy Dispersive X-ray (EDX), FT-IR and X-Photoelectron Spectroscopy (XPS) were used for detection structure, morphology, and size of a particle of Mn/CS nanocatalyst and mechanism of manganese onto copper slag. FESEM results show a good agreement with those determined by the XPS. Box–Behnken Design (BBD) was used for optimization of variables, such as gas flow rate (L/min), Temperature (°C), Reaction time (min) and SO_2 concentration (mg/L). Removal of SO_2 under the optimal conditions, (8.1414, 25, 60 and 3.94) for Gas flow rate, Temperature, Reaction time and SO_2 Concentration respectively were obtained. The most efficiency SO_2 removal achieved at the optimal operating conditions is around 99%. It is concluded that the usage of this photocatalytic oxidation of SO_2 process, can significantly reduce the SO_2 air pollution.*

KEYWORDS *Mn/Copper Slag; Catalytic oxidation; SO_2 oxidation; Column packed photocatalytic reactor; Nanocatalyst.*

INTRODUCTION

In recent years due to rapid industrial growth, increases the emissions of sulfur dioxide SO_2 and NOx. Air pollution is a growing hazard to human health and the natural environment. A most important air pollutant is SO_2 and emitted into atmosphere contamination impact on the environment such as acid rain and the photochemical smog, hazardous effects of the ecosystem, finally causing large harm to human health and the environment and accelerates the degradation and corrosion of buildings and structures [1]. It is recognized that SO_2 is not only harmful to human health but also carries the reactions that create an ozone reduction

***** *To whom correspondence should be addressed.*

+ *E-mail:* k-mahanpoor@iau-arak.ac.ir

1021-9986/2019/3/69-85 *17/$/6.07*

in the stratosphere and cause serious problems such as reduce ambient air quality and the environment, therefore played important role in the formation of haze [2]. Many developed countries need effectual methods of decreasing the amount of these gases. By the way; the SO_2 removal of various industrial sources has received much attention in the years [3]. Throughout the burning of fuels, many pollutants, including SO_2, NOx, and other hazardous gases are released. Commonly, SO_2 is controlled by oxidation and absorption, wet Flue Gas Desulfurization (FGD) methods [4-5]. The most common route for FGD method is scrubbing the polluted gas through alkali solvents similar urea, dilute sodium hydroxide, limestone slurries such as Wet limestone, gypsum Flue Gas Desulfurization (WFGD-Ca) and seawater [6]. UltraViolet (UV) irradiation, as an indirect non-thermal plasma method, is an important source of reactive species generation. The UV-induced oxidation, also known as PhotoChemical Oxidation (PCO), is safe and easy to apply. It has been widely used in environmental pollution control by advanced oxidation processes. Advanced Oxidation Processes (AOP) can produce hydroxyl radicals free to simultaneously oxidize and remove multiple pollutants from flue gas. Advanced Oxidation Processes (AOPs) can be extensively determined as aqueous phase oxidation methods based on the intervention in highly reactive species such as hydroxyl radicals in the removal of pollutants [7]. Therefore, developing more effective advanced oxidation flue gas purification technologies is still the main research subject in recent years. With such technologies, difficult compounds can be partially or fully oxidized into smaller products that can be easily removed from simpler biological processes [8]. A number of advanced oxidation processes, usually photo-oxidation [9], Sonochemical oxidation [10], adsorption removal [11] and Fenton oxidation [12], have been developed in the last several decades. The hydroxyl radicals generated in AOPs have been developed and used for removing various gaseous pollutants, such as SO_2, NO_X, trace elements, H_2S, and Volatile Organic Compounds (VOCs) in a short time and at ambient temperatures [13]. AOPs are capable of degrading almost all types of organic contaminants into harmless products and almost all related to the production of reactive hydroxyl radicals with a redox potential for 2.8 V [14]. In recent times Titanium dioxide based photocatalyst was reported in flue gas cleaning for emission control of SO_2 gas [15]. At present, there are studies related to evaluating the oxidation under the catalyst of phenol by means of the copper slag/H_2O_2 and copper slag/H_2O_2/UV systems for the depletion of organic contaminants [16]. The oxidation of SO_2 is an exothermic reaction and due to the negative reaction Enthalpy the equilibrium conversion decreases with rising temperature [17]. Copper slag is a byproduct obtained during the matte smelting and contains magnesium, iron oxide, and silica and copper slag catalysts are cheaper than nickel-based catalysts and non toxic [18]. In this sense, copper slag is an important co-product of the metallurgy industry that copper slag is mainly composed of Ferro silicate and magnetite [19]. At present, copper slag is developed and used in gasification as a catalyst action [20]. The Mn/CS is a good nanocatalyst for SO_2 photo oxidation catalytic at low temperatures. In this paper, a novel study on influences of Mn/CS and UV lamp power on SO_2 oxidation efficiencies was done in a CPPCR. The results will be able to give some theoretical instruction for development and application the SO_2 oxidation. The engineering problems are time-consuming and expensive. Therefore, novel statistical ways were used for solving difficult problems.

More recently additional techniques such as X-ray Photoelectron Spectroscopy (XPS), FESEM, XRD, and FT-IR have been used to surface chemical changes. The design of experiments can be useful to decrease the experimental number and introduce acceptable results [21]. RSM is a strong statistical based route for modeling complex systems and thus searching for the best conditions for desirable responses [22-23]. This study investigates the efficiency of AOP treatment using Box–Behnken design (BBD). Although several studies have been done on comprehending the oxidation of SO_2 with variety catalysts but as far we know this method hasn't been used and the advantage of this method in removing the gas is commodious and it decreases energy consumption in low temperatures. The presence of oxygen and water in the inlet stream increases the SO_2 adsorption capacity, due to the surface oxidation and the subsequent hydration to H_2SO_4. In this study, simple and highly effective oxidation using photo oxidation is presented. The goal of this work evaluates the potential use Mn/CS as a novel nanocatalyst for removal and oxidation of SO_2 from simulated flue gas using a conditions optimization by Box–Behnken design method.

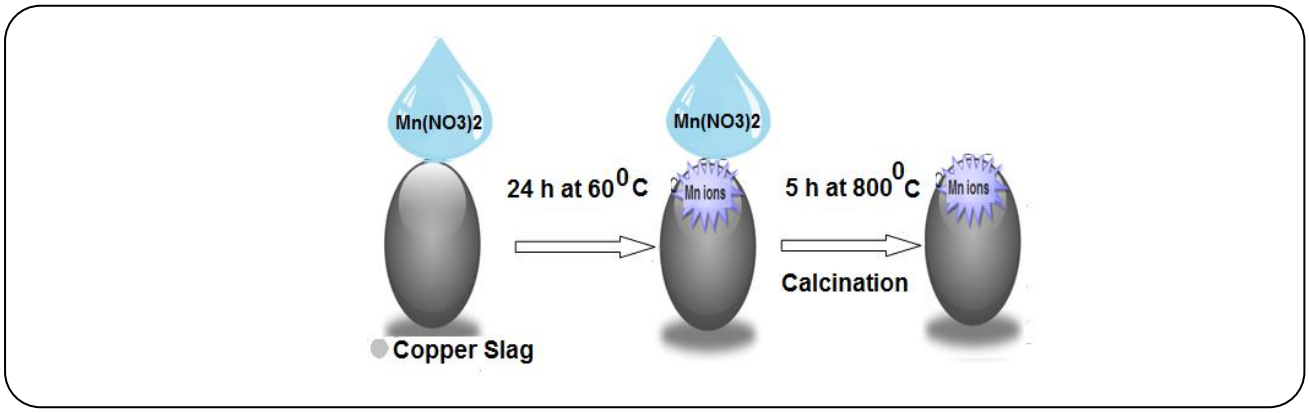

***Fig. 1:** Schematic of Fabrication of nanocatalyst Mn/copper slag.*

EXPERIMENTAL SECTION

Chemicals

Copper slag sample was purchased from Almahdi Kerman Company, Iran. The copper slag for a mean density of 3.5 g/cm^3 and particle size of the copper slag was well distributed within the range of 0.1 to 1.1 mm. Standard gases were used consist of N_2, O_2, SO_2 with purity (v/v) > 99.9%. All of gases were the products of the Gas Company, Iran. It should be noted that all the other reagents used were analytical grade such as Mn $(NO_3)_2$, NaOH, $BaCL_2$ and Calcium chloride was purchased from Merck Company for Purity >99%. All of them were the products of the Gas Company, Iran, were used to make the simulated flue gas and concentrations of the pollutants were regulated with the flue controllers.

Apparatus and software

FT-IR spectra were recorded by the FT-IR spectrometer (Perkin Elmer Spectrum Two American).

X-Ray Diffraction (DRD) tests were applied using a diffractometer (STOE STADI MP Model German).

The surface morphology of the samples was examined with a high resolution by Field Emission Scanning Electron Microscopy (FESEM) model (MIRA3-XMU-USA) set with energy dispersive X-ray (EDX) spectrometer.

Flue gas analyzer model KIGAZ 300 (Kimo Company, France, measuring range from 0 to 5000 ppm).

Conductometer instruments (Metrohm model 712).

A Thermo Bath lab-Companion model RW-0525G.

XPS was performed with a Thermo Scientific ESCALAB 250Xi using an Al Ka X-ray source (1486.6 eV).

UV lamp: 304 stainless steel body (model UV12GPM-55 watts, Philips).

Software Minitab Version (17), Statistica Version (10).

Fabrication of nanocatalyst

The Mn/CS has been prepared by two-step incipient wetness impregnation method; therefore ultra-pure water and a certain amount of copper slag slowly were added to a Mn $(NO_3)_2$ 50%solution (purchased from Merck Company) than being mixed and stirred in the beakers for 24h at 60^{0}C with heater stirrer. The schematic of Fabrication of nanocatalyst is shown in Fig. 1.

After extremely stirring the samples were dried at 80^{0}C for 12h in the oven and subsequently, the catalysts were calcinated in an electrical furnace at 800°C for 5 h. Finally, at 800°C for 5h, the Mn/CS was obtained [24].

Experimental procedures

The catalytic oxidation of SO_2 experiments was carried out as a pilot scale in a packed photocatalytic Reactor. In order to study experimentally was developed the oxidation of SO_2 and to determine numerically the efficiency an experimental setup as illustrated in Fig. 2. Main instruments showed the schematic of the set up a laboratory-scale in vertical, including three units: inlet simulated flue gas preparation sections, CPPCR the vertically and a flue gas analysis section respectively. The inlet gases consisted of three streams, i.e., nitrogen, sulfur dioxide and oxygen controlled in a flow controller. Three kinds of gases, N_2, O_2, and SO_2 with purity > 99.9% were used to make the simulated flue gas streams. The Pressure of gas and temperature preliminary were adjusted one bar and 25 °C respectively. The solubility of sulfur dioxide in water at a temperature 25°C is 0.724mmol/250 mL water. The inlet concentration of SO_2

(1) Thermo Bath	(6,8) Gas dryer
(2) Heat Exchanger	(7) Gas distributor
(3,5) separator	(9) Tail gas absorber
(4) Unite sampling outlet	(10)Flue Gas analyzer

Fig. 2: Schematic of experiments performed in a laboratory-scale system (Photo reactor).

according design of experimental was kept at between (2-10 mg/L), respectively. In addition, the effects of parameters on the performance of the SO_2 oxidation were also investigated. The flowing gases passing through a mixing chamber and inlet gases were injected to photoreactor by way counter current.

A flue gas stream, including sulfur dioxide is scrubbed with H_2O to dissolve sulfur dioxide. Solution temperatures adjusted to reactors and the temperature of solution monitored and controlled with thermo bath in the range (10-40^{0}C). The reactor with the volume of the reactor 5.3 Liter designed including a cylindrical stainless steel tube by the column length about 1160mm and was packed with Mn/CS. Fittings are employed to connect all parts of the apparatus. The flue gases fed from downstream to the photoreactor. The gas analyzer has a measuring range of 0-500 ppm and automatic zero and span calibration. The inlet concentrations of the pollutants were measured using the gas analyzer. The setup of experimental consists of (1) Thermo bath; (2) Heat exchanger;(3,5) Separator; (4) Unite outlets sampling; (6,8) Gas dryers;(7) Gas distributors;(9) Tail gas absorber;(10) Gas analyzer. A heat exchanger is near the CPPCR and the solution temperature is measured and adjusted by thermo bath. The gas flow rate in the dawn of reactors was controlled by a flow meter. The simulated flue gases to flow rate input (2-10 l/min) coupled with 2–10 mg/L SO_2 concentration. SO_2 was diluted with N_2 gas consequently the gases located and injected at the bottom of CPPCR. The catalyst was first exposed to the flue gas that contained 2–10 mg/L SO_2 gas via flow rate input (2-10 l/min). A UV lamp with 55 Watt, emitting at a wavelength of 254 nm was used as a light source and placed in vertical inside central part and protected with a quartz tube. A sample quartz tube with an external diameter of 34mm was placed within the center of the reactor (transition zone). The concentration of SO_2 was determined by a flue gas analyzer every 5min.

To do optimal conditions has tried to operate conditions, within the limits permitted sulfur dioxide in the air. The experiments were performed for the continued oxidation of SO_2 (2-10 mg/L) with ultrapure water at a liquid volume flow rate of 2.4 l/min through the circulation pump into the photoreactor via counter current to make the absorption of reaction between gas and liquid in the presence of Mn/CS. The flow rate of gas determines the time of adsorption between the gas and catalyst surfaces. With the decrease flow rate of gas a fewer number of SO_2 molecules contacted the surface of the catalyst.

The simulated flue gases with SO_2 passed through the inlet transition zone from the inlet to the reaction zone and perform the photo oxidation catalytic process. The reactor contains a fixed bed catalyst and from the reactor, the flow of gas-liquid passed during countercurrents. Often solid particles aren't to an extent but have a size distribution and larger particles are located at the bottom of the reactor. The solution flow rate of circulation was performed around 2.4 l/min between the storage tank and reactor. Column top pressure and column bottom pressure are (1-1.1atm) atmosphere respectively. Scrubbing solutions SO_2 will be released out of the solvent, whereas the lean solution in the bottom returns to the storage tank and through heat exchanger was adjusted, thus located at the top of the reactor with very little agitation of the liquid. The liquid stream would be fed to the reactor, to expand the catalyst bed, then UV lamp was turned thus measuring samples were used conductometric method [25]. Gas analyzers used to determine the outlet and inlet concentrations of pollutants. Each experimental run kept for 20-60 min on base experimental design. The concentration of SO_2 in outlet of photoreactor was recorded every 6 minutes. In this work, an analysis has been accomplished using conductometer with a detection limit of 0.001µS/cm-20 S/cm, was used to detect the conductivity of solutions. Moreover, it is easy to take samplings from the output of the CPPCR. In all experiments the dynamic capacity 650 g components (including about 400g of Mn/CS in constant and 250 g inert material) were packed in the photoreactor. In the case of the SO_2 concentration during the experiments were continuously monitored with a flue gas analyzer.

A separator polyvinyl chloride (PVC) body shown in Fig. 2 is usually vertical selected when the liquid /gas ratio is high. The gas dryers stainless steel body (6, 8), containing anhydrous calcium chloride as absorbent material is used for drying and purification of gas and the quality of the final products to ensure the measurement accuracy and the enhanced safety of electrochemical probes in flue gas analyzer (10). A gas analyzer with the ability for continuous measurements of SO_2, and O_2 from gas is used to measure the inlet and outlet concentrations of SO_2 pollutants. The residual pollutants in the exhaust protect the surrounding environment is used to with a tail gas absorber; contain 800 milliliters including solution of 0.2mol/L from NaOH, to reduce emission of pollution to the atmosphere. The gases were mixed in mixing chamber. The inlet and outlet concentrations of mixed gas were measured using gas analyzer and solution concentration perform with conductometric method. When the test finished, the gases were turned off.

Mechanisms of reaction

On the basis of the known results [26], there are three main removal pathways of pollutants using UV, UV/H_2O_2, AOP generally including the excitation removal of UV, the oxidation removal of H_2O_2, and the oxidation removal of $\bullet OH$ free radicals. Usually, the oxidation removal of $\bullet OH$ free radicals plays a leading role among them. Interaction between gases ant catalyst in mechanisms of reaction plays an important role in the performance of SO_2 oxidation via nano catalyst because of the shape of the Mn/CS. The SO_2 oxidation H_2SO_4 can occur either in the gas phase or in the aqueous Phase. The convert SO_2 to SO_3 which are the chemical species such as O_2used to be oxidized thus showed in the following reactions [27]. These [reactions (1)-(10)] were shown that a Mn ion was loaded on the surface of copper slag. In this mechanism, $h\vartheta$ causes the SO_2, to transfer to an electronically excited state. In addition, SO_2 can react with Mn particles on the catalyst surfaces that results in an interference with SO_2 oxidation. On the other hand, when UV is added (turning on the UV lamp), a lot of $\bullet OH$ free radicals are produced by photo oxidation of H_2O according to the following reaction(3-4). The photo oxidation catalytic in the present of hydroxyl free radicals was performed in the following below reactions. The liquid-phase oxidation of SO_2 through atmospheric oxygen in the presence of Mn/CS catalyst was performed

SO_4^{2-} mainly. As a result, catalytic oxidation processes are performed by reactant adsorption, conversion, and desorption respectively. Based on the experimental results and pervious reported characterization, the proposed reaction mechanism in Mn/CS photocatalytic oxidation system for SO_2 removal is illustrated and proposed and the results are shown in Fig. 3 and Eqs. (1)- (10). UV irradiation can generate active radicals •OH, using nanocatalyst. SO_2, O_2, and H_2O first adsorb on the surface of the catalyst and then react to form adsorbed H_2SO_4. Sulfuric acid is formed when oxygen and water are injected into the Column. All these suppositions are summarized in the following sequence of reactions that try to explain the mechanism of SO_2 removal by Mn/CS catalyst.

$$Mn/CS + h\vartheta \rightarrow Mn/CS^*\left(h^+ + e^-\right) \quad (1)$$

$$h^+ + e^- \left(\text{recombined}\right) \rightarrow \text{heat} \quad (2)$$

$$h^+ + H_2O \rightarrow \bullet OH + H^+ \quad (3)$$

$$h^+ + OH^- \rightarrow \bullet OH \quad (4)$$

$$O_2 + e^- \rightarrow \bullet O_2^- + H_2O \rightarrow \bullet OOH + OH^- \quad (5)$$

$$2 \bullet OOH \rightarrow O_2 + H_2O_2 \quad (6)$$

$$e^- + H_2O_2 \rightarrow \bullet OH + OH^- \quad (7)$$

$$SO_2 + 2 \bullet OH \rightarrow SO_3 + H_2O \quad (8)$$

$$SO_2 + \bullet O_2^- + H_2O \rightarrow SO_3 + 2OH^- \quad (9)$$

In the meantime, the SO_3 existing in the gas stream also dissolves into the aqueous solution:

$$SO_3 + H_2O \rightarrow H_2SO_4 \quad (10)$$

Based on the electron-hole mechanism have produced hydroxyl free radicals. It is known that t $\bullet OH$ is the main radical species for SO_2 oxidation because of its large rate constant K = 7.5 $\times 10^{-2} cm^3$/Molecule.s in comparison with those of other radical species [28]. These results indicated that the Mn/CS has higher photocatalytic oxidation activity in the presence of UV. In this case, the anions are completely separated, due to pKa value very large and consequently.

The oxidation of SO_2 on the surface of catalyst consists of fundamentally different processes and interactions that occur on Mn/CS. During the reaction is a proton is released because the concentration of all the species are low and the molar conductivity of $H^+$is further than the rest of the ions, on the other hand the oxidation of SO_2 can be connected to the change in conductivity. The conductivity of the SO_2 aqueous solution was carried out at various concentrations with a conductivity of SO_2 aqueous.

Data processing

The average conductivity within 60 min measured by the final solution is used as the outlet conductivity of SO_2 in the aqueous phase.

The conductivity of the SO_2 aqueous solution was carried out at various concentrations with conductometric sensing.

The SO_2 removal efficiency was calculated using the following Eq. (11). Where η (%) is the SO_2 oxidation efficiency, which is used as the dependent variable, EC_{in} is the initial conductivity of SO_2 aqueous solution, 0.570 mS/cm; EC_{fi} is the final or outlet conductivity of the aqueous solution.

$$SO_2 \text{oxidation efficiency}\left(\%\right)\eta = \frac{\left|EC_{in} - EC_{fi}\right|}{EC_{in}} \times 100 \quad (11)$$

Photocatalytic oxidation and Conductivity Control

The performance of the nanocatalyst for photocatalytic oxidation of SO_2 was performed in a CPPCR. Before testing the oxidation of SO_2 through photocatalytic oxidation; experiments were performed in order to clearly demonstrate the measure the absorption of SO_2 in the CPPCR. The experiments firstly were carried out in the condition dark (without UV), and the inlet and outlet materials were measured. Without photo oxidation alone was achieved near 20% SO_2 oxidation efficiency. The major idea of our experiment for the preparation of the novel nanocatalyst is an inexpensive and simple route. On the other hand the SO_2 oxidation reaction easily has been performed under novel nanocatalyst at aqueous solution. SO_2 was shown to have serious negative effects on the catalyst surface due to the reaction between SO_2 and Mn/CS active sites, as determined by XRD and FT-IR results.

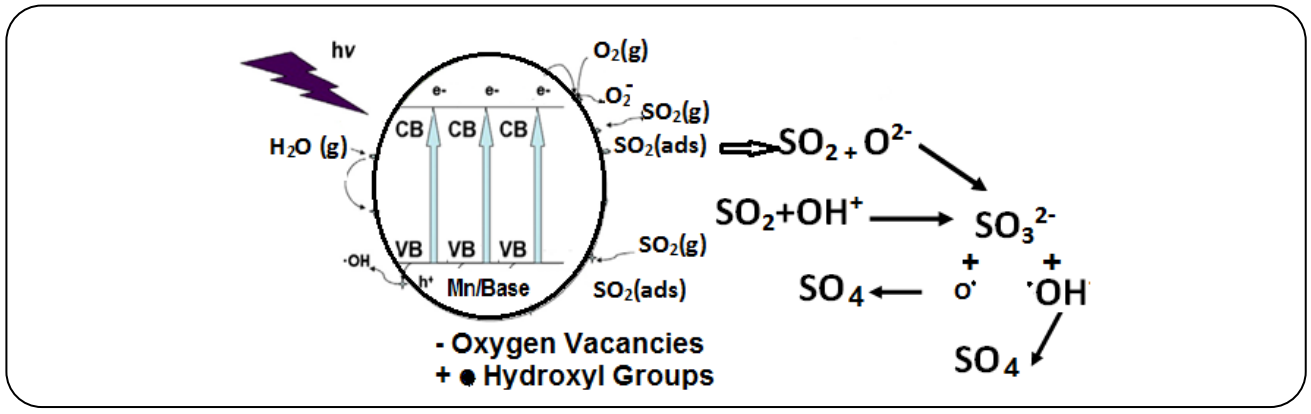

Fig. 3: The Proposed mechanism illustrating the action of the Ultraviolet induced photocatalysts for the oxidation of SO_2.

Response Surface Methodology

In this study optimization of control factors was performed using RSM. RSM is an improvement of mathematical and statistical techniques useful for the modeling [29]. In this study, the optimization of experimental conditions for the oxidation of SO_2 gas via Mn/CS was carried out at various using Box–Behnken Design (BBD) technique. The Box–Behnken (BBD) is a useful route in response surface methodology that a quadratic model for the variable. RSM is a congregation of statistics for the developing, filtration and optimizing processes. The consequence of independent variables and their interactions were investigated by ANOVA. The performance or quality is known as the response. A three level, four factors, by a Box–Behnken designs were determined for further optimization for each variable; three levels were designed and coded with (-1, 0, +1). The Box–Behnken is a high quality design in the sense that it could be fitted in the quadratic model. In the running experiments, with the Box–Behnken design and the RSM the effects of the four independent variables on the response functions and to find the optimal conditions were investigated [30]. Among all the RSM designs, Box–Behnken designs to require fewer runs the mathematical relationship between the response (Y) and the independent variables (X) can be approximated by a quadratic polynomial equation as follows:

$$Y = \beta_0 + \sum \beta_i X_i + \sum \beta_{ii} X_i^2 + \sum\sum \beta_{ij} X_i X_j + \varepsilon \qquad (12)$$

Where, Y indicates the predicted response, β_0 is a constant β_i , β_{ii} and β_{ij} are the linear, quadratic and interaction influences and ε is the random error which shows the different sources of variability. The coefficients of the response functions of different dependent variables were determined to correlate the experimental results with the response functions using a Box–Behnken design. In order to estimate the regression coefficients, a number of experimental design techniques are available. It should be noted; however, also no replication is needed to find error mean square. The error mean square can be found out by replicating the central points [31]. The good quality of the models was judged over their coefficients of correlation and determination. The fitness of each model was checked with the analysis of variance. To determine the relationship between the response factor and a subset of the independent factors the statistical significance of the model and the coefficient were analyzed by means of F-test and P-value respectively.

RESULTS AND DISCUSSION

Nanocatalysts characterization

X-ray diffraction (XRD)

The XRD analysis was applied to investigate the chemical composition and structure of copper slag, Mn/CS. Analysis of XRD can be utilized to measure peaks broadening with crystallite size [32]. XRD analysis was performed through *cuka* radiation. The data that shows intensity is plotted in a graph based on 2Theta on a range of 10–90 degrees. A typical XRD pattern of the nanocatalyst of Mn/CS as illustrated in Fig. 4. The peaks centered on 2θ of 24.30, 28.5, 35.28, 44.97, 51.55 and 66.5. As can be seen, in Fig. 4, XRD analysis showed that the catalyst Mn/CS prepared by the impregnation method well matched with the H-copper slag. This indicates that the framework structure of copper slag is unaltered

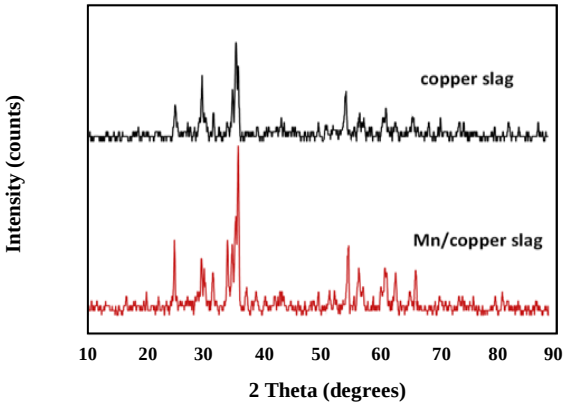

Fig. 4: XRD patterns of the Copper Slag and Mn/Copper Slag nanocatalyst.

during the impregnation process. Impregnation is an alternative treatment that has received significant consideration recently for the oxidation of SO_2. Crystallites proportions of Mn/CS have important implication in inter crystalline dispersion rates of molecules as well as in the contribution to the outer surface area to reaction rates and indicated that the Manganese particles were incorporated into the copper slag structure. The average crystallite size of the prepared Mn/CS was estimated by applying the Debye Scherer's equation [32].

$$d = \frac{k\lambda}{\beta \cos\theta} \qquad (13)$$

Where d is the crystallite size to be calculated, k equal 0.9 and β is the Full Width at Half Maximum (FWHM) of the peak, λ is the wavelength of X-ray corresponding to the cuka radiation (0.154056 nm) and 2θ is the Bragg angle. It is well-known that the Mn/CS establishes with an average crystallite size of about 68.43 nm.

Energy–dispersive X-ray spectroscopy

The EDX spectrum of copper slag and Mn/CS nanocatalyst are depicted in Fig. 5, Using the result of the Energy dispersive X-ray spectroscopy (EDX) analyses show that the amount of manganese fixed on copper slag is equal to 11.37 Wt%. Thus the EDX confirmed the coating of manganese on the copper slag and results are shown in Fig. 5.

Field Emission Scanning Electron Microscopy

As can be seen from Fig. 5, the morphologies of the Mn/CS were evaluated by FESEM equipped with EDX. The chemical compositions of copper slag are shown in Fig. 5. The copper slag surface morphology and size of it before and after the stabilization of manganese was identified with copper slag and Mn/CS, respectively. As seen in these image particle sizes that located on the catalyst, the surface is not equal and structure of these particles is crystalline. Also was increased porosity on the surface of catalyst Mn/CS.

FT-IR spectroscopy

The FT-IR spectra of the studied samples are presented in Fig. 6 and Table 1. It is noted that copper slag FT-IR spectrum in the wave number ranges between 400-4000 cm^{-1} with a resolution of 4 cm^{-1} with accumulating 32 scans were studied. The wave numbers accuracy is 0.01 cm^{-1} and the sampling resolution was 0.09 cm^{-1}, in this method; functional groups were identified in the copper slag. Around 3950 cm^{-1} a peak exhibited the hydrate such as Mn $(OH)_2$ and the peak around3530 cm^{-1} shows the S-O stretch such as $MnSO_4$. The peak of around1592 cm^{-1} relates to the C-O asymmetric stretching, whereas a peak at1408 cm^{-1} may be due to the bonding in the carbonate ions, indicating the presence of some carbonated minerals, possibly due to the adsorption of CO_2 from the atmosphere. The obtained FT-IR spectra of copper slag samples corresponded almost entirely to the spectrum of the tephroite phase (α-Mn_2SiO_4). This made possible the use of FT-IR to determine the composition of tephroite through the established dependency on spectrum bands positions on tephroite composition. Adsorption wave's number in the spectrum determines the chemical structure of the copper slag. The broad absorption bands of the range of 3100-3600 cm^{-1} are corresponding to the O–H stretching vibration of water that with the samples was adsorbed. As shown in Fig. 6 the Characteristic FT-IR spectra according to Mn contents in Tephroite structure (Mn_2SiO_4) were appearing in 900-1000 cm^{-1} IR bond [33]. This band represents the main stretching vibrations of different OH^- groups present in Mn–OH–Al, Al–OH–Al, and Fe–OH–Al units in the octahedral layer therefore because sulfur dioxide is an acid gas, active sites accountable for adsorption should have a basic structure [33]. After nanocatalyst preparation, the wave number is shifted from 610 to 640 cm^{-1}. The IR bands of the amorphous SiO_2 are at 1101, 971and 801 cm^{-1} [34]. The Si-O-Si

Table 1: FT-IR spectrum the copper slag and Mn/Copper Slag.

Copper slag		Mn/Copper Slag	
Wave number (cm^{-1})	Assignment	Wave number (cm^{-1})	Assignment
3436.5	O-H stretching, vibration in Si-OH	3435.96	O-H stretching, vibration in H_2O
1630	O-H bending vibration in Si-OH	1367	Mn-O-H bending vibration
977, 990	Si-O asymmetric stretching, vibration in SiO_4	978,933,902	Si-O asymmetric stretching vibration
592	C-O vibration	697	Mn-O stretching vibration
1101,971	Si-O asymmetric deformation, vibration in SiO_4, Si-O-symmetric stretching vibration in SiO_4	1101,971	Si-O asymmetric deformation, vibration in SiO_4units, Si-O symmetric stretching, vibration in SiO_4 units, Mn-O deformation vibration

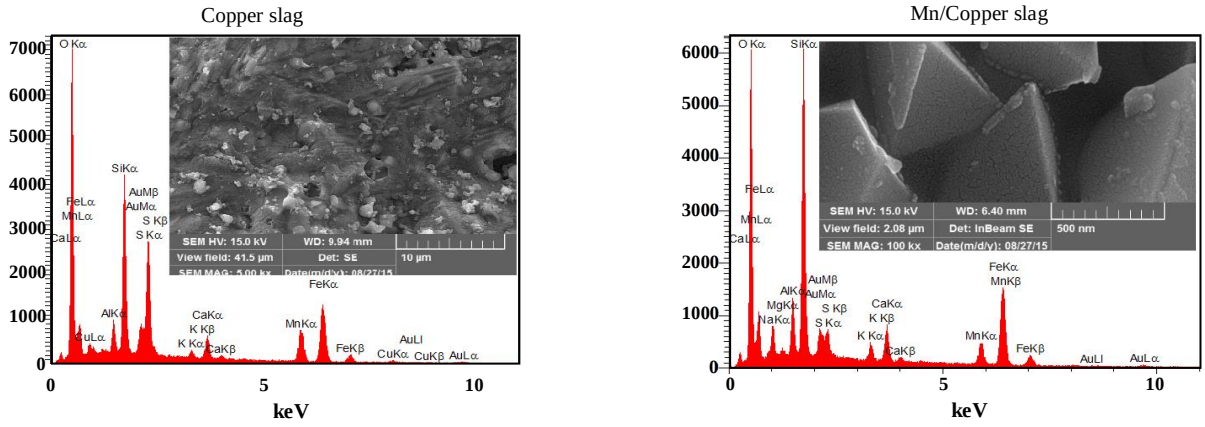

Element	Percent	O	Al	Si	S	K	Ca	Mn	Fe	Cu
Copper slag	Wt.%	38.72	1.45	9.63	6.42	0.51	1.94	5.76	18.16	3.09
	Atomic%	61.34	1.36	8.67	5.07	0.33	1.22	4.17	8.23	1.24
Mn/copper slag	Wt.%	41.76	1.63	8.03	7.22	0.65	2.14	11.37	16.35	1.12
	Atomic%	66.16	1.53	7.23	5.70	0.42	1.35	8.23	7.41	0.45

Fig. 5: FESEM images, Copper Slag and Mn/Copper Slag and EDX elemental analysis spectrum of the samples of Copper Slag and Mn/Copper Slag.

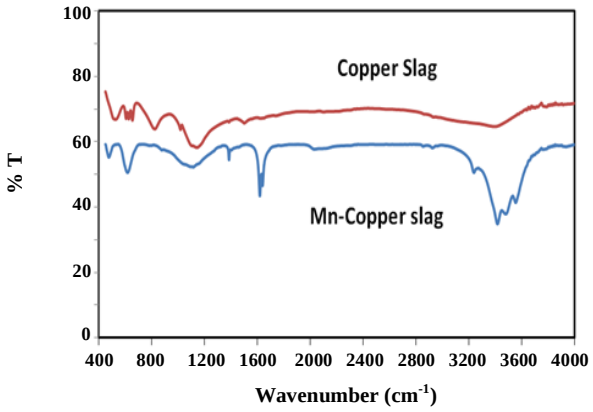

Fig. 6: FT-IR spectra of the studied materials: copper slag and Mn/Copper Slag.

stretching band of bulk silica is prominent at 1116 cm^{-1}, while the Si-O stretch of silanol groups of the silica surface can be seen at 980 cm^{-1} mainly $MnSO_4$, in agreement with data from XRD Fig. 4. Three absorption features due to water can be assigned to the OH stretching modes 3000-3600 cm^{-1}, H-O-H bending mode 1637 cm^{-1}, and an arrangement band 2130 cm^{-1}. The FT-IR results have proven that Mn as well as placed on the surface of the copper slag.

XPS studies

XPS experiment has been operated to study the detail structure information of Mn/copper slag. XPS modeling gives a relationship between the thicknesses and

Table 2: Experimental range and levels of independent variables.

Independent variables	Range and levels		
Variables	Level 1 (-1)	Level 2 (0)	Level 3 (+1)
Gas flow rate (l/min) (x_1)	2	6	10
Temperature (^{0}C) (x_2)	10	25	40
Reaction time (min) (x_3)	30	45	60
SO_2 concentration (mg/l) (x_4)	2	6	10

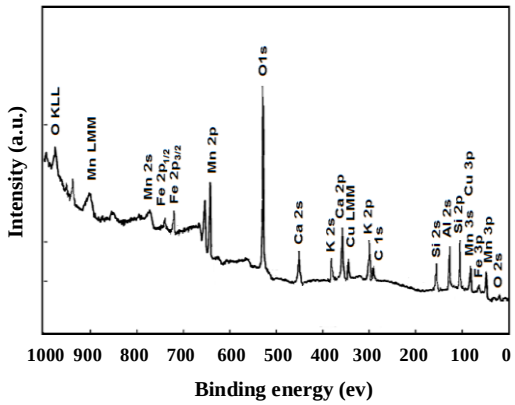

Fig. 7: X-ray photoelectron spectrum of the Mn/Copper Slag nanocatalysts.

the covering of the deposited thin film. Moreover, manganese was detected on the copper slag surface by XPS measurement. Therefore, the Si2s photoemission peaks is recorded (Fig. 7).The fitting shows the presence of two peaks at 153 eV and 173.4 eV which are ascribed to the Si-Si and Si-O bonds, respectively. Moreover the 20.4 eV shift between the two peaks indicate the SiO_2 stoichiometry of the native oxide. XPS of Mn (2s) region is also shown in Fig. 7 of the Supporting Information. The Mn (2s) peak appearing around 786.1 eV is typical of intercalated Mn ions in copper slag layers.

Box-Behnken design

In this study Minitab software was used to develop optimal oxidation of SO_2 based on the Box–Behnken design with four variables is shown in Table 2. In this study, the optimization of experimental conditions for SO_2 oxidation using the conductivity method was studied using Box–Behnken design under RSM. In order to clearly demonstrate the calculate the influence of operating parameters on the SO_2 oxidation, four main factors of three levels, each one was chosen: Gas flow rates (l/min)(x_1), Temperature (^{0}C) (x_2), Reaction time (min) (x_3) and SO_2 Concentration (mg/L) (x_4). As shown in Table 2 at three levels lower (-1), medium (0) and high (+1) each variable was studied. A Box-Behnken design was selected to study the influences of four influencing variables on the oxidation efficiency. Table 3 presents the experimental design matrix, the values, and response for the experiments. In all, 27 experiments were conducted in triplicate and all results obtained from the Box–Behnken design is summarized in Table 3. A total of 27 experiments is employed in this work to evaluate the influences of the four main independent parameters on SO_2 oxidation efficiency.

Model equation

The experiment results in conjunction with the design matrix are shown in Table 3. It was found that the relationship between SO_2 oxidation efficiency and the four operating parameters (i.e., Gas flow rate (l/min) (x_1), Temperature (^{0}C) (x_2) Reaction time (min) (x_3) and SO_2 Concentration (mg/l) (x_4)) was fitted to a second-class polynomial equation. The final mathematical equation in terms of the actual factors (confidence level above 95%) was determined by BBD is given below:

$$\eta = +1.688 + 4.7943x_1 + 3.2834x_2 + 0.5696x_3 + \quad (14)$$
$$6.1981x_4 - 0.2955x_1^2 - 0.0675x_2^2 - 0.3977x_4^2 - 0.052x_3x_4$$

The SO_2 removal efficiency was calculated using the following Eq. (14). Where η (%) is equal to the SO_2 oxidation efficiency, which is used as the dependent variable and the second-order polynomial equation relating the response.

Analysis of variance (ANOVA)

A statistical technique is ANOVA that classification all variations on a set of data into parts associated

Table 3: Factor levels for a Box-Behnken design of a four variable system.

	Actual values				Oxidation Efficiency η (%)		
Observation -Run	x_1	x_2	x_3	x_4	$\eta_{experimental}$	$\eta_{predicted}$	Residual
1	2	10	45	6	71.00	70.93	0.07
2	10	10	45	6	80.90	80.91	-0.01
3	2	40	45	6	68.00	68.07	-0.07
4	10	40	45	6	78.00	78.05	-0.05
5	6	25	30	2	84.35	84.51	-0.16
6	6	25	60	2	98.60	98.54	0.06
7	6	25	30	10	83.50	83.69	-0.19
8	6	25	60	10	85.53	85.50	0.03
9	2	25	45	2	81.81	81.80	0.01
10	10	25	45	2	91.80	91.78	0.02
11	2	25	45	10	74.91	74.87	0.04
12	10	25	45	10	84.85	84.86	-0.01
13	6	10	30	6	76.62	76.69	-0.07
14	6	40	30	6	73.83	73.83	0.00
15	6	10	60	6	84.67	84.61	0.06
16	6	40	60	6	81.61	81.75	-0.14
17	2	25	30	6	80.77	80.74	0.03
18	10	25	30	6	90.90	90.72	0.18
19	2	25	60	6	88.59	88.67	-0.08
20	10	25	60	6	98.52	98.65	-0.13
21	6	10	45	2	77.71	77.75	-0.04
22	6	40	45	2	75.00	74.89	0.11
23	6	10	45	10	70.80	70.82	-0.02
24	6	40	45	10	68.11	67.96	0.15
25	6	25	45	6	94.45	94.42	0.03
26	6	25	45	6	94.50	94.42	0.08
27	6	25	45	6	94.51	94.42	0.09

for testing hypotheses on the parameters of the model. The quality of the fit of the l model is expressed by (R^2) and is checked by the F-value (Fischer variation ratio) and p-value or the same significant probability value. The model terms are selected on the probability value of 95% confidence intervals. To study the influence of four independent variables (x_1, x_2, x_3, and x_4) on the characteristics of SO_2 oxidation and efficiency, ANOVA was performed; whereby significant oxidation of SO_2 during the reactions was introduced under optimal conditions are shown in Table 4. As be seen in Table 4 Suitability of the model was tested using analysis of variance. The model F values of 22645.78 and p-values less than 0.05 indicated that the models are significant for SO_2 oxidation. Adjusted R^2 measures the amount of variation explained in the form after adjusting

Table 4: ANOVA results of the response surface quadratic model.

ANOVA test for response function						
Source	DF	SS	MS	F-value	P-value	Remarks
Model	8	2123.29	265.41	22645.78	0.0001	Significant
Linear	4	655.83	163.96	13989.47	0.0001	Significant
x_1	1	298.9	298.9	25503.22	0.0001	Significant
x_2	1	24.51	24.51	2091.29	0.0001	Significant
x_3	1	188.42	188.42	16076.35	0.0001	Significant
x_4	1	144.01	144.01	12287.01	0.0001	Insignificant
Square	3	1430.13	476.71	40674.36	0.0001	Significant
$x_1 \times x_1$	1	134.17	134.17	11447.93	0.0001	Significant
$x_2 \times x_2$	1	1386.94	1386.94	118338.22	0.0001	Significant
$x_4 \times x_4$	1	242.99	242.99	20732.73	0.0001	Significant
2 Way Interaction	1	37.33	37.33	3185.3	0.0001	Significant
$x_3 \times x_4$	1	37.33	37.33	3185.3	0.0001	Significant
Error	18	0.21	0.01		0.0001	Significant
Lack of Fit	16	0.21	0.01	12.07	0.079	Insignificant
Pure Error	2	0	0			
Total	26	2123.5				

for the number of parameters in it. The high value of adjusted R^2 indicated the higher fitness of the model.

In this study, the value of $R^{2,}$ adjusted R^2 and predict R^2 were 0.9999, 0.9999 and 0.9997, respectively. The low probability (<0.05) with F-value (22645.78) implied that the model was correct.

The influence of experimental conditions on SO_2 oxidation efficiencies

In this work, to see the effect of effect of parameters on the oxidation efficiency, response surface plots are useful for the model equation image and perceiving the nature of response surface. Fig. 8, shows the response surface plots of SO_2 oxidation efficiency (%) using BBD. Fig. 8(a), shows the consequence of SO_2 concentration on the removal efficiency. When the SO_2 concentrations were increased, SO_2 removal efficiency was improved. It recognized that oxidation efficiency increased with the decreasing of SO_2. The removal efficiency of SO_2 roughly decreased with the increase of inlet concentration of SO_2.The influence of reaction temperature on the removal efficiency was shown in Fig. 8 (c). When the reaction temperatures were increased, SO_2 removal efficiency was improved. It demonstrated that the oxidation efficiency increased primary and when the reaction temperature was higher than 25°C, the SO_2 oxidation efficiency decreased rapidly. When the flow rates were increased, SO_2 removal efficiency was improved. It can be seen from Fig. 8b; the gas flow rate increased from 1 L/min to 10 L/min SO_2 removal efficiency was increased. The low removal efficiencies were obtained due to the low production of reactive oxygen species with short irradiation time or low power UV lamp under fast flow rate conditions. It demonstrated that the photocatalytic oxidation efficiency, increasing with the increasing of reaction time and Flow rate gas was shown in Fig. 8 (b).

Accurately model

The results were analyzed using the Anova a regression model, the coefficient of resolve (R^2), adjusted R-square and response plots. The Anova is a usual

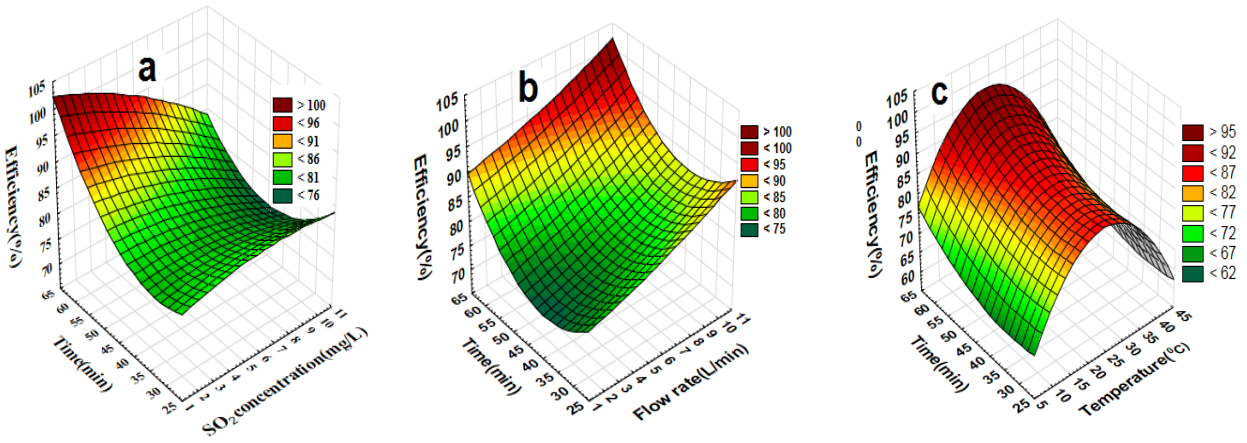

Fig. 8: Surface plots for the effects. (a) Response surfaces plot for interaction SO_2 concentration and Reaction of time. (b) Response surfaces plot for interaction Flow rate and Reaction of time. (c) Response surfaces plot for the interaction Temperature Reaction of time.

the statistical route in the different fields. The Anova provides a statistical process that determines whether the means of several groups are equal or not. The F-value of 22645.78 ultimately demonstrates that the model is significant. In addition, the P-value of the model is less than 0.05, representing that it is a significant and desirable model. Enough to represent the real relationship between the response efficiency and the significant variables, with a very small P-value (0.0001) and satisfactory coefficient of designation (R^2 =0.99). According to Table 4, SO_2 concentration is the most effective individual factor of SO_2 oxidation. Fig 9 (d) shows the plot the predicted values of the experimental values. The normal probability plots (NPPs) and residuals plot for SO_2 oxidation are shown in Figs (9a) - (9d) respectively. In this, all of Figs. 9 are shown a behavior observed in the real value of efficiency. In this case, the normal probability of residuals plot (Fig. 9a) is straight that implies a satisfactory normal distribution and the independence of the residuals and this (Fig. 9a) display the same trend of behavior observed in the actual value of data's effects on SO_2 oxidation. The optimal level of key factors and their interaction effects on SO_2 oxidation was investigated through the Box–Behnken design of the RSM. Interaction influences of variables can be expected from the outputs of experimental design which is the major reason for doing experimental design. Based on the resulted model Eq. (14), it was found that reaction time had no significant influence on the SO_2 oxidation. Among parameters in the model, x_4 with the highest coefficient value (6.1981) was shown a larger effect on SO_2 oxidation efficiency. Table 5 shows the observed and predicted values. The residuals against experimental runs were analyzed by creating the rewarding fit of the model and indicates that all the data points place within the limits Fig. 9 (e). Based on Fig. 9 (e), the suitable fitness between experimental data and predicted values could be revealed.

The results of the experiments performed demonstrated that the main products formed in the oxidation of SO_2 in atmospheric oxygen in Mn/CS nanocatalyst were obtained barium sulfate. As four factors with the software of Minitab optimized for the oxidation of sulfur dioxide have been reported are shown in Table 5.

Fig. 10 represents the breakthrough curves for SO_2 oxidation in different reaction systems. As shown in Fig. 10, the SO_2 only achieves a removal efficiency of 1% in the single UV system and when the single copper Slag system, are used alone to remove the SO_2, respectively, there is almost no SO_2 removed, but using the UV/(Mn/Copper Slag) AOP system achieves an SO_2 removal efficiency of 99.0%. The oxidation removal of $\bullet OH$ free radicals plays a leading role (it has a share of 80.2%). In summary, on the basis of our results, although several other side reactions can also possibly occur in the solutions, the main removal path of SO_2 can be briefly

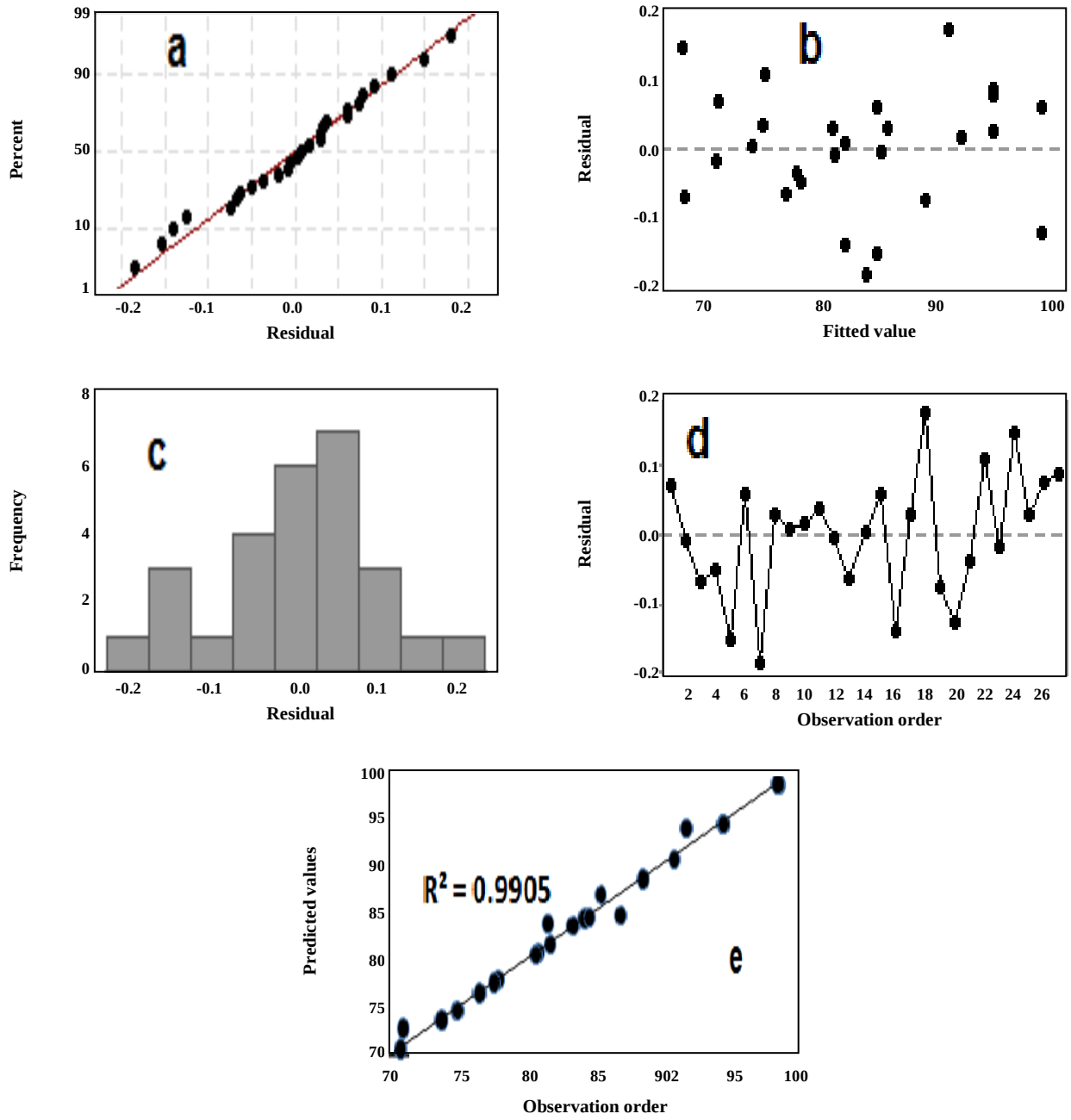

Fig. 9: Residual plots of SO_2 oxidation. (a) Normal% probability plots of the residuals, (b) residual values versus Fitted Value (c) The plot of residuals of frequency (d) Plot of residuals versus observation (e) Comparison between the curve of experimental response and predicted response.

illustrated by Eqs 1-10. In addition, the removal of SO_2 by Mn/CS was carried out under the optimal conditions, in which, the optimal conditions, for gas flow rate, was 8.1414 (l/min) Temperature25 (^{0}C), Reaction time 60 min and SO_2 Concentration 3.94 mg/L respectively were obtained removal efficiencies of SO_2(99.9%).

CONCLUSIONS

Our investigation has demonstrated the high importance of a catalytic oxidation SO_2 study in optimal conditions, which has not been reported previously. In this research, we proposed the feasibility of the novel catalytic oxidation process with Mn/CS nanocatalyst

Table 5: The optimum conditions of BBD.

Gas flow rate (l/min)	Temperature (^{0}C)	Reaction time (min)	SO_2 concentration (mg/L)
8.1414	25	60	3.94

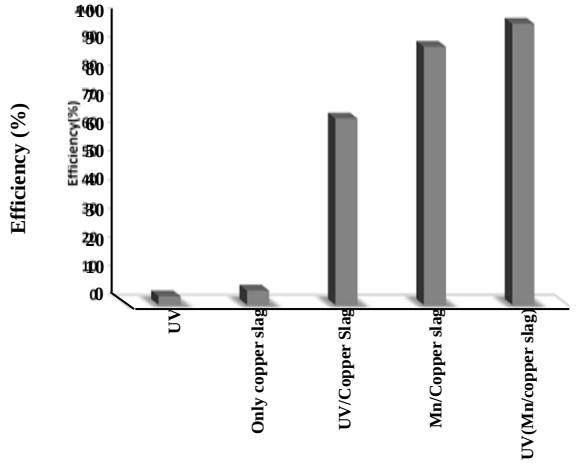

Fig. 10: Breakthrough curves for efficiencies of SO2 oxidation in different reaction systems. Conditions: Gas flow rate (8.1414(l/min)), Solution Temperature 25 °C, Reaction time (60min) and SO_2 Concentration3.94mg/L.

under UltraViolet (UV) irradiation, successfully and cost-effectively for photocatalytic oxidation of SO_2 from simulated flue gas. Characteristics, structural change of the samples in copper slag and Mn/copper slag have been investigated by XRD, FTIR, EDX, FESEM and XPS spectra.

In this regard, with four independent variables, Gas flow rate, Temperature, Reaction time and SO_2 Concentration were optimized based on BBD. The Mn/CS successfully was synthesized using the impregnation method for photo oxidation of SO_2 in the simulated flue gas. This study was applied to aiming at obtaining high oxidations and maximizing productivity. The results were optimized about similar for both models. The higher catalytic activity of Mn/CS, as novel process was developed for removal of SO_2 in liquid phase. Removal of SO_2 under the optimal conditions (8.1414(L/min), 25°C, 60 min and 3.94 mg/L) for gas flow rate, Temperature, Reaction time and SO_2 Concentration respectively were obtained. FT-IR, XRD, XPS, EDX, FESEM analysis showed that Mn/CS was successfully used to be applied as nanocatalyst for oxidation of SO_2. Thus, XPS shows that the deposited copper slag is organized as a good base. Some useful conclusions are obtained and summarized as follows:

1-using BBD optimization, the oxidation efficiency achieved for SO_2 was 99%.

2- In low temperatures of Mn/CS nanocatalyst done a significant role in the removal of sulfur dioxide.

3-with increase in temperature of operations, SO_2 oxidation efficiency first increased reaches 25 °C and then decreased.

4- The reactor contains a fixed bed catalyst and from the reactor, the flow of gas-liquid passed through counter-currents. Often solid particles were not to an extent, but have a size distribution and larger particles are located at the bottom of the reactor.

5-Remarkable advantages of this nanocatalyst are the simple synthesis procedure, high catalytic activity, easy separation, and acceptable reusability. The excellent correlation between predicted and observed oxidation efficiency and significance $R^2 = 0.99$ and $R^2adj = 0.999$ values were obtained in the optimal conditions that giving good accordance between the model and experimental results.

6- This study demonstrates that UV irradiation can remove SO_2 effectively, and the final product would be H_2SO_4.

7-Under all experimental conditions, the SO_2 was completely removed. On the basis of Mn/CS nanocatalyst, a new process was developed for removing SO_2, in the liquid phase. Under the optimal conditions, the removal efficiencies of 99% for SO_2.

The results given in this paper can be usefully applied for the industrial application of FGD systems in the removal of SO_2, which could be helpful for optimizing the SO_2 pollution control.

Acknowledgments

The authors wish to thank the Islamic Azad University of Arak, Iran for financial support.

Received : Sep. 5, 2017 ; Accepted : Apr. 23, 2018

REFERENCES

[1] Shokri A., Rabiee F., Mahanpoor K., Employing a Novel Nanocatalyst (Mn/Iranian hematite) for Oxidation of SO_2 Pollutant in Aqueous Environment, *Int J Environ Sci Technol*, **14**: 2485–2494 (2017).

[2] Liu y., Wang y., Xu W., Yang W., Pan Z., Wan Q., Simultaneous Absorption–Oxidation of Nitric Oxide and Sulfur Dioxide Using Ammonium Persulfate Synergistically Activated by UV-Light and Heat, *Chem. Eng. Res Des*, **130**: 321–333 (2018).

[3] Ding J., Zhong Q. ,Zhang S., Song F., Bu Y., Simultaneous Removal of NO_X and SO_2 From Coal-Fired Flue Gas by Catalytic Oxidation-Removal Process with H_2O_2 ,*Chem Eng J*, **243**: 176-182 (2014).

[4] Hao R., Zhao Y., Yuan B., Zhou S., Yang S., Establishment of a Novel Advanced Oxidation Process for Economical and Effective Removal of SO_2 and NO, *J. Hazard. Mater*, **318**: 224–232 (2016).

[5] Sun, C., Zhao N., Zhuang Z., Wang H., Liu Y., Weng X., Wu Z., Mechanisms and Reaction Pathways for Simultaneous Oxidation of NOx and SO_2 by Ozone Determined by in Situ IR Measurements, *J. Hazard. Mater*, **274**: 376–383 (2014).

[6] Darake S., Hatamipour M. S., Rahimi A., Hamzeloui P., SO_2 Removal by Seawater in a Spray Tower: Experimental Study and Mathematical Modeling, *Chem Eng Res. Des*, **109**: 180–189 (2016).

[7] Yarahmadi R., Mortazavi S.B., Omidkhah M.R., Asilyan H., Moridi P, Examination of the Optimized Conditions for the Conversion of NO_X Pollution in DBD Plasma Reactor, *Iran. J. Chem. Chem. Eng. (IJCCE)*, **28**: 133-140 (2010).

[8] Almomani F.A., Bhosale R.R., Kumar A., Kennes C., Removal of Volatile Sulfur Compounds by Solar Advanced Oxidation Technologies and Bioprocesses, *Sol. Energy*, **135**(1): 348–358 (2016).

[9] Liu Y., Wang Q., Yin Y., Pan J., Zhang J., Advanced Oxidation Removal of NO and SO_2 Fromflue Gas by Using Ultraviolet/H_2O_2/NaOH Process, *Chem Eng Res Des*, **92**: 1907–1914(2014).

[10] Zhou T., Zou X., Wu X., Mao J., Wang J., Synergistic Degradation of Antibiotic Norfloxacin in a Novel Heterogeneous Sonochemical Fe^0/Tetraphosphate Fenton-Like System, *Ultrason Sonochem*, **37** : 320–327(2017).

[11] Bao J., Dai Y., Liu H., Yang L, Photocatalytic Removal of SO_2 over Mn Doped Titanium Dioxide Supported by Multi-Walled Carbon Nanotubes, *Int. J. Hydrogen Energy*, **41**: 15688–15695 (2016).

[12] Shokri A., A Kinetic Study and Application of Electro-Fenton Process for the Remediation of Aqueous Environment Containing Toluene in a Batch Reactor, *Russ j Appl Chem*, **90**: 452–457 (2017).

[13] Liu Y.X., Zhang J., Photochemical Oxidation Removal of NO and SO_2 from Simulated Flue Gas of Coal-Fired Power Plants by Wet Scrubbing Using UV/H_2O_2 Advanced Oxidation Process, *Ind. Eng. Chem. Res*, **50**: 3836–3841 (2011).

[14] Hao R., Yang S., Zhao Y., Zhang Y., Yuan B., Mao X., Follow-up Research of Ultraviolet Catalyzing Vaporized H_2O_2 for Simultaneous Removal of SO_2 and NO: Absorption of NO_2 and NO by Na-Based WFGD Byproduct (Na_2SO_3), *Fuel Process. Technol*, **160**: 64–69 (2017).

[15] Nasonova A., Kim K.S., Effects of TiO_2 Coating on Zeolite Particles for NO and SO_2 Removal by Dielectric Barrier Discharge Process, *Catal. Today*, **211**:90–95 (2013).

[16] Huanosta-Gutiérrez T., Dantas R.F., Ramírez-Zamora R.M., Esplugas S., Evaluation of Copper Slag to Catalyze Advanced Oxidation Processes for the Removal of Phenol in Water, *J. Hazard. Mater*, **214**: 325–330 (2012).

[17] Benzinger W., Wenka A., Dittmeyer R., Kinetic Modelling of the SO_2-Oxidation with Pt in a Microstructured Reactor, *Appl. Catal. A Gen*, **397**: 209-217 (2011).

[18] Zhang F.X., Hu J.H., Yang B., Yu Y.N., Syngas Production from Biomass Gasification Using Copper Slag Catalysts, *Adv. Mater. Res*, **725**: 313–318 (2013).

[19] Sarfo P., Das A., Wyss G., Young C., Recovery of Metal Values from Copper Slag and Reuse of Residual Secondary Slag, *Waste Manage*, **70**: 272-281(2017).

[20] Deng S., Hu J., Wang H., Li J., An Experimental Study of Steam Gasification of Biomass over Precalcined Copper Slag Catalyst, *Adv Mater Ress*, **638**: 479–489 (2013).

[21] Bakhtiari G., Bazmi M., Abdouss M., Royaee S.J, Adsorption and Desorption of Sulfur Compounds by Improved Nano Adsorbent: Optimization Using Response Surface Methodology, *Iran. J. Chem. Chem. Eng. (IJCCE)*, **36**(1): 69-79(2017).

[22] Shokri A., Mahanpoor K, Soodbar D, Evaluation of a Modified TiO_2 (GO–B–TiO_2) Photo Catalyst for Degradation of 4-Nitrophenol in Petrochemical Wastewater by Response Surface Methodology Based on the Central Composite Design, *J. Environ Chem. Eng*, **4**: 585–598 (2016).

[23] Keypour H., Noroozi M., Rashidi A., Shariati Rad M., Application of Response Surface Methodology for Catalytic Hydrogenation of Nitrobenzene to Aniline Using Ruthenium Supported Fullerene Nanocatalyst, *Iran. J. Chem. Chem. Eng. (IJCCE)*, **34**(1): 21-32 (2015).

[24] Shi J., Yao L., Hu C., Effect of CO_2 on the Structural Variation of Na_2WO_4/Mn/SiO_2 Catalyst for Oxidative Coupling of Methane to Ethylene, *J. Energy Chem*, **24**: 394-400 (2015).

[25] Tanvir N.B., Yurchenko O., Laubender E., Pohle P., Sicard O.V., Urban G., Zinc Peroxide Combustion Promoter in Preparation of CuO Layers for Conductometric CO_2 Sensing, *Sens. Actuators, B: Chem.*, **257**: 1027-1034 (2018).

[26] Liu Y., Wang Q., Zhang J., Simultaneous Removal of Hg^0 and SO_2 from Flue Gas Using Vacuum Ultraviolet Radiation Combining with Absorption of Urea Solution, *Int. J. Coal Geol*, **170**: 41-47 (2017).

[27] Su C., Ran X., Hu J., Shao C., Photocatalytic Process of Simultaneous Desulfurization and Denitrification of Flue Gas by TiO_2- Polyacrylonitrile Nano Fibers, *Environ. Sci. Technol*, **47**:11562−11568 (2013).

[28] Sun C., Zhao N., Zhuang Z., Wang H., Liu Y., Weng X., Wu Z., Mechanisms and Reaction Pathways for Simultaneous Oxidation of NOx and SO_2 by Ozone Determined by in Situ IR Measurements, *J. Hazard. Mater.*, **274**: 376–383 (2014).

[29] Zhao C., Liu J., Li Z., Li F., Tu H., Sun Q., Liao J., Yang J., Yang Y., Liu N., Biosorption and Bioaccumulation Behavior of Uranium on Bacillus sp.dwc-2: Investigation by Box-Behenken Design Method, *J. Mol. Liq.*, **221**:156-165 (2016).

[30] Nam Nam S.N., Cho H., Han J., Her N., Yoon J., Photocatalytic Degradation of Acesulfame K: Optimization Using the Box–Behnken Design (BBD), *Process. Saf. Environ. Prot.*, **113**: 10–21 (2018).

[31] Goleij M., Fakhraee H., Response Surface Methodology Optimization of Cobalt (II) and Lead (II) Removal from Aqueous Solution Using MWCNT-Fe_3O_4 Nanocomposite, *Iran. J. Chem. Chem. Eng. (IJCCE)*, **36**: 129-141 (2017).

[32] Khorsand Zak A., Majid W.H.A., Ebrahimizadeh Abrishami M., Yousefi R., Parvizi R., Synthesis, Magnetic Properties and X-Ray Analysis of $Zn_{0.97}X_{0.03}O$ nanoparticles (X = Mn, Ni, and Co) using Scherrer and Size-Strain Plot Methods, *Solid State Sci.*, **14**: 488–494 (2012).

[33] Potysz A., Kierczak J., Fuchs Y., Grybos M., Guibaud G., N.L. Lens p., D.van Hullebusch E., Characterization and pH-Dependent Leaching Behaviour of Historical and Modern Copper Slags, *J. Geochem. Explor.*, **160**: 1-15 (2016).

[34] Guo Q., Huang D., Kou X., Cao W., Li L., Ge L., Li J., Synthesis of Disperse Amorphous SiO_2 Nanoparticles Via Sol–Gel Process, *Ceram. Int.*, **43**: 192–196 (2017).